RESEARCH PAPER

Electrowetting valves for sweat-based microfluidics

Aditi R. Naik[1] · Brenda Warren[1] · Andrew Burns[2] · Ralf Lenigk[2] · Jeffrey Morse[1] · Azar Alizadeh[2] ·
James J. Watkins[1]

Abstract
Skin-compatible microfluidic valving systems with on-demand sweat capture are necessary to understand the temporal variation of biomarkers. Here, we demonstrate solution-based electrowetting valves with rapid actuation integrated into a flexible microfluidic sweat collection patch. The valve is produced by inkjet-printing a pair of silver electrodes with spacings of 0.2–2 mm and modifying the downstream electrode with a hydrophobic self-assembled monolayer. To complete the valve, a microfluidic channel is fabricated from laser ablation of adhesive layers and pressed over the silver electrodes. Artificial perspiration is driven by capillary action within the channel until stopped by the electrowetting valve. A low voltage is applied to the electrodes, decreasing the surface energy of the hydrophobic monolayer and allowing the fluid front to continue through the microchannel. Statistical analysis demonstrated that applied voltage, and not electrode spacing, influenced valve actuation time, with 17 ± 8 s for 4 V and 40 ± 16 s for 1 V. Inkjet-printing conditions were also optimized to achieve a valve fluid retention time of 9 h. Using four electrowetting valves, an integrated wearable device is designed for artificial perspiration collection through valve actuation at distinct time points over 40 min. Finally, these inexpensive, user-friendly, and disposable electrowetting valves offer exciting opportunities for non-invasive point-of-care sweat monitoring.

1 Introduction

Wearable sweat sensing devices are emerging as a topic of interest for inexpensive point-of-care diagnostics (Jadoon et al. 2015; Koh et al. 2016; Bariya et al. 2018). Sweat is secreted from the eccrine glands and is composed primarily of water and a mixture of electrolytes, proteins, and biomolecules that contain valuable information regarding overall health status. Compared with blood, urine, and tears, sweat is a biofluid that offers the potential for non-invasive continuous monitoring of significant biomarkers over extended periods of time (Bandodkar and Wang 2014; Heikenfeld

---

✉ James J. Watkins
watkins@polysci.umass.edu

1 Department of Polymer Science and Engineering, University of Massachusetts, Amherst, MA 01003, USA

2 General Electric Global Research Center, Niskayuna, NY 12309, USA

2016). Recently, several innovative wearable sweat sensors using electrochemical and colorimetric analysis approaches have demonstrated the feasibility and importance of these types of devices (Gao et al. 2016; Alizadeh et al. 2018; Choi et al. 2019; Kim et al. 2020). On demand sweat collection at distinct time points is yet another key capability, which would allow for assessment of temporal variation of health biomarkers. In particular, hydration is an essential indicator of overall health and performance and is measureable through detection of the major sweat electrolytes (Na+, K+, and Cl−). Continuous measurements of hydration level through sweat sensing would be of importance to several population groups, including athletes, military personnel, elderly people, and medical patients, and would serve as an early dehydration warning to prevent injury, illness, or death. (Coyle et al. 2009; Baker 2017; Alizadeh et al. 2018; Seshadri et al. 2019). Therefore, it is of great interest to develop a scalable, adaptable, and disposable microfluidic valve for sweat collection.

The electrowetting valve is flexible, solution-based, low-power, and reliable microfluidic system with demonstrated potential for point-of-care diagnostics as shown by Merian

et al. (2012). Electrowetting is used for a wide variety of applications, including electrowetting pumps (Mach et al. 2002), pixel displays (Shamai et al. 2008), microconveyors (Moon and Kim 2006), dynamic lensing (Hendriks et al. 2005), electronic paper (Di et al. 2015), and digital microfluidics (Atabakhsh and Jafarabadi Ashtiani 2018; Guo et al. 2019; Tohgha et al. 2019; Torabinia et al. 2019). The electrowetting-on-a-dielectric concept used for this valve is described by a change in surface energy of a thin hydrophobic insulator coated over a conductive material by applying a potential through an electrolytic solution (Quilliet and Berge 2001). The electrowetting valve consists of two parallel electrodes inkjet-printed across a microfluidic channel with a hydrophobic self-assembled monolayer deposited on the electrode downstream from the fluid inlet. An electrolyte solution is introduced into the microchannel and driven by capillary action without the need for an external pumping system. The fluid front is prevented from further flow by the hydrophobic electrode. The valve is opened by applying a low voltage to both electrodes, resulting in an electrowetting-on-a-dielectric actuation mechanism on the hydrophobic electrode. This simple valve requires no external moving parts and extends the ability for capillary-flow driven microfluidics to include timed delivery of fluids for complex measurements. Electrowetting valves are used in lateral flow assays and microfluidic chips for the detection of food-borne pathogens, such as rRNA (Koo et al. 2013), T7 bacteriophages (He et al. 2014), and Salmonella (Chen et al. 2015). Additionally, electrowetting valves require low power and are amenable to roll-to-roll processing, allowing for large-scale and low-cost manufacturing (Chen et al. 2015).

To use electrowetting valves for sweat-sensing applications requires further optimization of the valve development and design. As discussed in previous literature, electrowetting valves use a minimum electrode spacing of 0.45 mm, require an actuation voltage of 2 V (He et al. 2014) and prevent fluid flow for approximately an hour (Chen et al. 2015). Sweat sensing applications will require lower voltages to reduce external power requirements and prevent the electrolysis of water, which produces bubbles within the microchannel. Valve fabrication should additionally involve a hydrophilic substrate to wick sweat through the microchannel and a skin adhesive for wearable applications. Therefore, an electrowetting valve developed for sweat sensing applications remains a significant challenge.

Here, we demonstrate the fabrication of wearable electrowetting valves with fast and reliable actuation at low voltages for sweat-based microfluidic devices. Through optimized processing conditions, we have achieved valve actuation at voltages as low as 1 V, electrode spacings as small as 0.2 mm, and fluid retention times of 9 h. Furthermore, multiple electrowetting valves are demonstrated to open individually from a single connected hydrophilic electrode, decreasing the dimensions of the overall valving system. As a proof-of-concept device, a wearable patch using four electrowetting valves is developed to collect artificial perspiration over specific time points. These results will allow for the integration of low-cost, portable, and scalable electrowetting valves for point-of-care microfluidics requiring the precise control of sweat capture for continuous biomarker measurements.

2 Materials and methods

2.1 Inkjet printing of silver ink

The printed silver electrodes for electrowetting valves were fabricated using nanoparticle-based silver ink (Metalon JSB-25HV, Novacentrix), which contained 25 wt% silver in an aqueous dispersion. Prior to printing, the ink was filtered through a 1 μm polytetrafluoroethylene filter (Whatman, GE) and pipetted into a 10-pL ink cartridge. The Dimatix DMP-2850 (Fujifilm) inkjet printer was used to print the silver electrode patterns directly onto a polyethylene terephthalate (PET) film (Novele, Novacentrix). During printing, four nozzles, a customized waveform (see Fig. S1), and 28 V jetting voltage were used with a cleaning cycle every 25 s. The printed silver ink was annealed at 130 °C for 5 min until conductive. For improved valve fluid retention times, the electrodes were printed orthogonal to the direction of fluid flow within the microchannel.

2.2 Valve electrode fabrication

To produce the electrowetting valve, two separate silver electrodes were necessary: a hydrophobic and a hydrophilic electrode. The first silver electrode was printed, annealed, and modified with a silane for the surface to become hydrophobic. Then the second silver electrode was printed and annealed, remaining hydrophilic.

For the hydrophobic electrode, the annealed silver was exposed to UV Ozone (Model 42, Jetlight Company, Inc.) treatment for 15 min to remove surface contaminants. The silver electrode was immersed in a 12 mM solution of 1H, 1H, 2H, 2H-perfluorodecanethiol (PFDT, Sigma-Aldrich) in ethanol (Pharmco-Aaper) for 30 min under gentle agitation. This silanization technique was modified from previous literature (He and Nugen 2014). The electrode was then rinsed with ethanol to remove excess PFDT and dried under nitrogen. The hydrophilic electrode was produced by inkjet-printing the silver ink parallel to the hydrophobic electrode using a fiducial mark to create the desired distance between the two electrodes. Silver connectors were printed

simultaneously with the electrodes to provide connection points for the external power supply.

2.3 Microfluidic assembly and testing

A microfluidic system was assembled over the two electrodes to complete the electrowetting valve for testing and validation. Pressure-sensitive adhesive (PSA, ArCare 92,712) of 48 um thickness was lasercut (VLS3.50, Universal Laser Systems) to fabricate a 2 mm wide microchannel. Inlet and outlet ports for the microchannel were cut from Tegaderm (3M), a transparent medical-grade skin adhesive using a hollow punch with 3 mm diameter. The PSA microchannel was adhered to the Tegaderm and then to the PET layer to minimize damage to the printed electrodes. One drop (~ 50 µL) of artificial perspiration (Pickering, pH 4.5) mixed with blue food dye (McCormick) was pipetted over the inlet of the microfluidic device, which was closest to the hydrophilic electrode. The blue dye does not affect the electrowetting valve actuation and can result in a color gradient due to diffusion through the microchannel (He and Nugen 2014). To actuate-to-open, wires were connected to a power supply box (80 W Switching DC Power Supply, Extech) and clipped to the silver electrodes. The voltages used for actuation were between 1 and 4 V and the current was set to 0 A for all experiments. The positive potential was applied to the hydrophilic electrode, and the negative potential to the hydrophobic electrode.

2.4 Analysis techniques

Several characterization techniques were used to examine the printed electrowetting valves. Optical microscopy (OM, Zeiss Axio Scope A1) was used to observe the drop size spacing of the printed silver and distance between the electrowetting valve electrodes. Scanning electron microscopy (SEM, FEI Magellan 400 XHR) and energy-dispersive X-ray spectroscopy (EDS, FEI Magellan 400 XHR) were used to characterize the surface of the printed silver electrodes. Mechanical profilometry (Dektak 150, Veeco) was used to measure the height profile of the 20 µm drop size spacing printed silver electrode. The four-point resistivity system (Signatone) was used to measure the sheet resistivity of the printed electrode patterns at different drop size spacing. The video contact angle system (VCA Optima, AST Products, Inc) was used to measure the static contact angles of water on the printed and modified silver surfaces. Origin Pro 9 (OriginLab, Northampton, MA) was used for the statistical analyses.

3 Results and discussion

The fabrication of wearable electrowetting valves for sweat-sensing applications is outlined in Fig. 1a. The valve consists of two silver electrodes inkjet-printed onto a flexible hydrophilic PET substrate. First, the electrode downstream from the fluid inlet is printed and modified to be hydrophobic by depositing a self-assembled monolayer of PFDT. Next, a second electrode is printed parallel to the modified hydrophobic electrode and termed hydrophilic. Finally, PSA with a 2 mm wide lasercut microchannel and a conformal medical-grade skin adhesive are assembled over the printed electrodes, completing the valve. As shown in Fig. 1b, c, valve actuation is due to electrowetting-on-a-dielectric when a potential difference is applied across the two electrodes. For this effect to occur, both the hydrophobic electrode coated with PFDT and the hydrophilic electrode must be
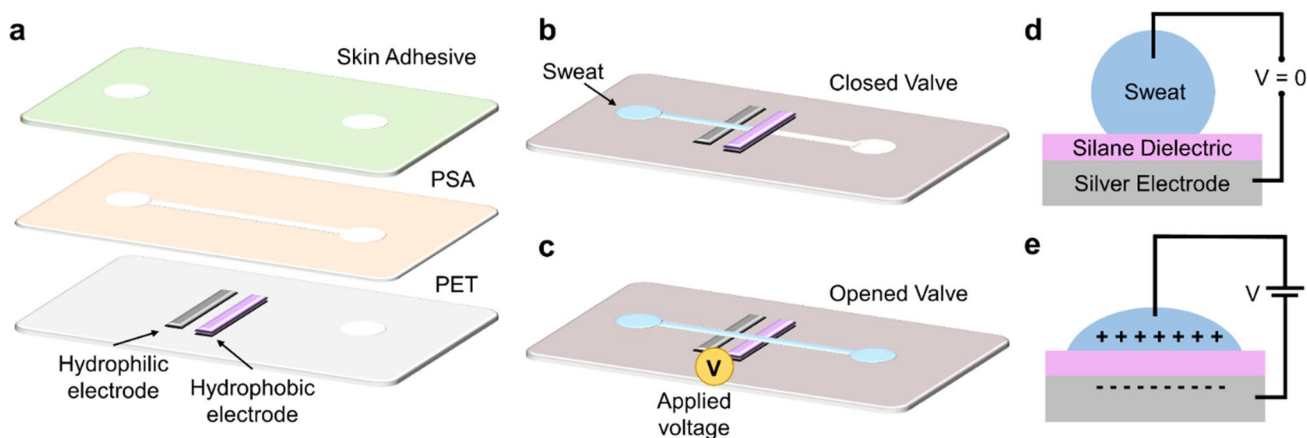
Fig. 1 Schematic of electrowetting valve fabrication and actuation. **a** Wearable electrowetting valve assembly, including inkjet-printed hydrophilic and hydrophobic electrodes on PET, PSA microchannel, and skin adhesive. **b** Closed and **c** opened electrowetting valve. **d** Electrowetting-on-a-dielectric representation of a droplet of sweat over a hydrophobic silane dielectric and conductive silver electrode before and **e** after voltage application

in direct contact with sweat within the microchannel. The droplet of sweat serves as the electrolytic solution, containing ions of sodium, chloride, potassium, magnesium, and calcium (Gao et al. 2016; Anastasova et al. 2017). Applying a potential across the electrodes and sweat droplet results in a voltage-dependent reduction in the interfacial surface energy of the hydrophobic electrode, shown in Fig. 1d, e, opening the valve and allowing fluid to flow forward through the channel (Liu et al. 2010; Mugele and Baret 2005).

3.1 Inkjet printing optimization

Robust electrodes with excellent print quality are necessary to fabricate reliable electrowetting valves that remain closed for several hours and actuate-to-open when desired. It is important that the printed silver electrodes demonstrate high electrical conductivity, strong substrate adhesion without crack formation or delamination, and high hydrophobicity following monolayer deposition. Novacentrix JSB-2HV silver nanoparticle-based ink satisfied these criteria when printed on Novacentrix Novele PET. This water-based ink consisted of 25 wt% silver content with a viscosity of 8–10 cP and surface tension of 30–32 dyne/cm as provided by the supplier. The inkjet-printing conditions were optimized to produce uniform ink droplets and minimize satellite droplets during printing. A voltage of 28 V was applied to four sequential print nozzles using an optimized jetting waveform and a cleaning cycle every 25 s.

Five different drop size spacings (15, 20, 25, 30, 35 μm) were examined to determine the printed resolution required for the valve electrodes. Optical microscopy images of the print quality and the resistivity versus drop size spacing are shown in Fig. S2. A drop size spacing of 20 μm (1270 dpi) demonstrated low sheet resistivity after annealing without ink pooling (Fig. S2a) or gaps between printed lines (Fig. S2f and S2e). These types of printing defects resulted in delamination of the electrodes during the hydrophobic modification step and increased resistivity. The conductivity for silver ink printed at 20 μm drop size spacing was measured to be $8.8 \times 10^2 \pm 0.1 \times 10^2$ S/m, based on the electrode
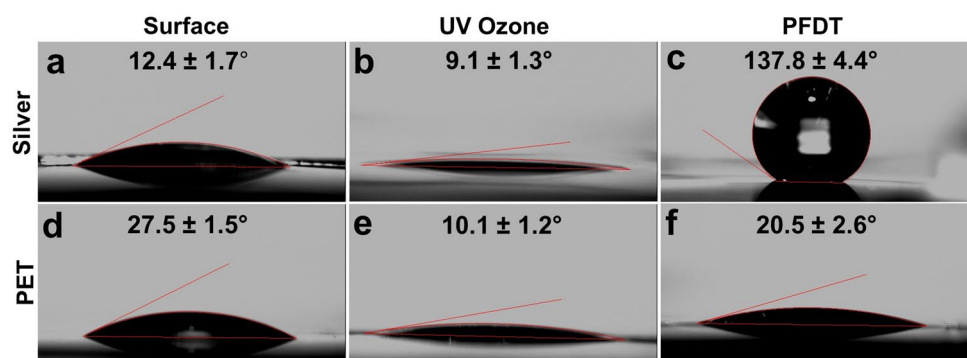
thickness (see Fig. S3) of 1.6 ± 0.1 um. Good adhesion between the printed silver and the PET substrate was demonstrated in Fig. S4.

3.2 Hydrophobic electrode modification

Prior to PFDT modification, the silver electrodes were treated with UV Ozone to reduce contaminants on the surface and increase wetting behavior as shown in Fig. 2a, b (He et al. 2014). Previous electrowetting studies demonstrated immersion deposition resulted in higher hydrophobicity compared with drop-casting directly onto the silver.(He and Nugen 2014) Therefore, electrodes were immersed in 12 mM PFDT/ethanol solution for 30 min under gentle agitation, achieving a static contact angle of $138 \pm 4°$ as shown in Fig. 2c. The contact angle was measured in both the parallel and perpendicular direction of printing and found to be similar. The immersion time was determined by assessing the contact angle following PFDT modification every five minutes as shown in Fig. S5. The advancing contact angle was measured to be $161 \pm 4°$, as shown in Fig. S6. Furthermore, this modification technique decreased the immersion time required as compared to the 3 h immersion time when using a 2 mM PFDT solution, as discussed in previous literature (Merian et al. 2012; He and Nugen 2014). As a note, a self-sintering ink was also considered for rapid electrode fabrication; however, the additional additives in the ink were suspected to have decreased available PFDT reaction sites, resulting in lower hydrophobicity. Furthermore, the PFDT-modified electrode is expected to remain thermally stable at body temperature (Chandekar et al. 2010).

It is also necessary to demonstrate that the PET substrate remained hydrophilic following the PFDT modification step. The increased wetting capability the PET substrate would allow for capillary-driven flow to wick sweat quickly from the skin into the microchannel without the need for an external pump. The second electrode, referred to as the hydrophilic electrode, is aligned parallel to the hydrophobic electrode and printed. As shown in Fig. 2d, f, the contact angle of the substrate following modification is similar to

Fig. 2 PFDT Modification. Static contact angle of **a–c** silver electrode surface and **d–f** PET substrate following UV Ozone treatment and PFDT immersion, respectively

	Surface	UV Ozone	PFDT
Silver	**a** 12.4 ± 1.7°	**b** 9.1 ± 1.3°	**c** 137.8 ± 4.4°
PET	**d** 27.5 ± 1.5°	**e** 10.1 ± 1.2°	**f** 20.5 ± 2.6°

the untreated substrate. Therefore, the same inkjet printing conditions discussed previously were used to produce the second hydrophilic electrode.

The printed silver electrodes were characterized by scanning electron microscopy (SEM) and energy-dispersive X-ray spectroscopy (EDS) as shown in Fig. 3. The silver nanoparticles in the printed ink coalesced to form a conductive film following a 5 min thermal annealing step at 130 °C. The silver surface showed an increased microscale roughness after UV Ozone treatment to remove contaminants and lower surface energy. EDS was performed to ensure that the PFDT monolayer was uniformly coated over the silver surface during the immersion step. Elemental analysis of the printed electrode prior to modification demonstrated predominantly silver, as shown in Fig. S7. In comparison, the silver modified with PFDT confirmed the presence of fluorine covering the electrode surface.

Furthermore, it is necessary that the hydrophobic electrode prevent fluid flow for several hours prior to actuation of the valve by applied voltage. Previous electrowetting valve literature demonstrated fluid retention time ranging from 15 min to approximately 1 h before undesired flow (Koo et al. 2013; Chen et al. 2015) To increase the retention time, the printing direction of the electrode was explored with respect to fluid flow. A microchannel was assembled over a hydrophobic electrode printed orthogonal to and in-line with the direction of fluid flow as shown in Fig. S8. Artificial perspiration with blue dye was pipetted into the 3 mm diameter inlet port, allowing the sweat to wick towards the hydrophilic electrode with a width of 0.5 mm. The electrodes printed orthogonal to the direction of sweat flow demonstrated retention times greater than 9 h, while electrodes printed in-line with the direction of flow showed times less than 3 h. This difference is a result of the ~500 nm thin fluid pathways formed due to inkjet-printing from neighboring nozzles. These printing artefacts are noticeable in the electrode height profile in Fig. S3. The hydrophobic electrode fabrication was thus optimized and characterized with regard to inkjet-printing conditions, PFDT modification, and print direction.

3.3 Valve assembly and actuation

To fabricate the electrowetting valve, the hydrophilic electrode was aligned alongside the hydrophobic electrode using a fiducial mark and printed on the PET substrate. The two electrodes were annealed at 130 °C for 5 min to allow the hydrophilic electrode to become conductive. The PFDT monolayer on the hydrophobic electrode is thermally stable until 145 °C and is not damaged during this annealing step. The hydrophobic electrode was printed at a width of 0.5 mm and the hydrophilic at 1 mm with four increasing spacings between the electrodes: 0.2, 0.5, 1, and 2 mm, to examine the effect of electrode spacing on actuation time. A 2 mm-wide microchannel backed with a skin adhesive was assembled over the two electrodes to complete the valve as shown in the optical microscopy images in Fig. 4.

The actuate-to-open time was evaluated with regard to the four electrode spacings using applied voltages of 1–4 V as shown in Fig. 5a. This electrowetting valve study is the first to demonstrate reliable actuation at 0.2 mm electrode spacing and an applied voltage of 1 V (Merian et al. 2012). Electrowetting valves were also opened using an applied voltage of 0.5 V; however, the actuation times showed a large variation and were not reproducible for all samples. To actuate, a negative potential is applied to the hydrophobic
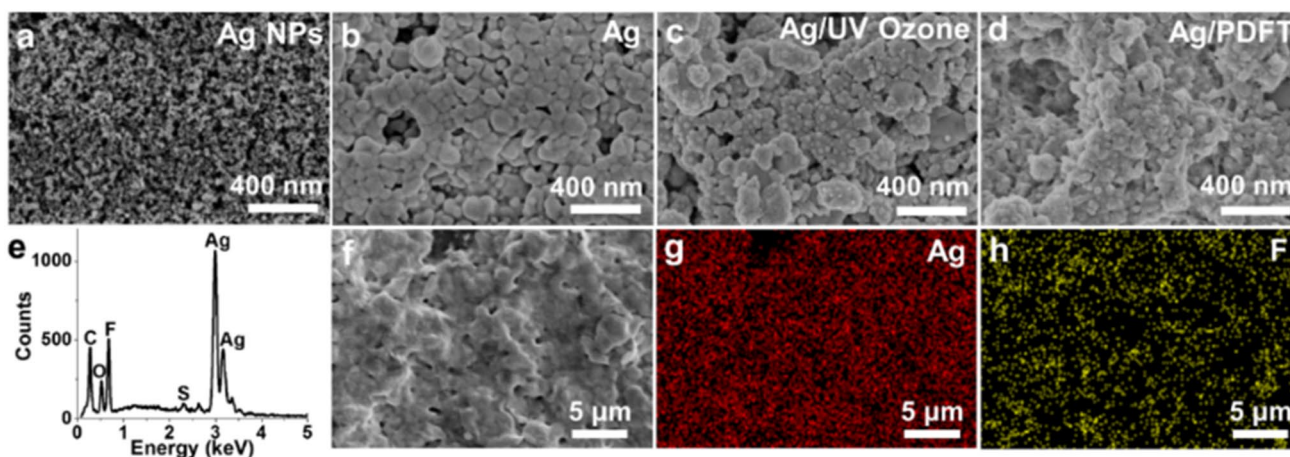

Fig. 3 Electrode surface characterization. High-resolution SEM images of **a** inkjet-printed silver nanoparticle ink following **b** thermal annealing, **c** UV Ozone treatment, and **d** PFDT deposition. Scale bar is 400 nm and samples were coated with 2 nm Pt for imaging. **e** EDS spectrum showing elemental peaks for silver, fluorine, sulfur, carbon, and oxygen. **f** SEM image of silver after PFDT deposition on Si substrate and elemental mapping of **g** silver and **h** fluorine. Scale bars are 5 μm
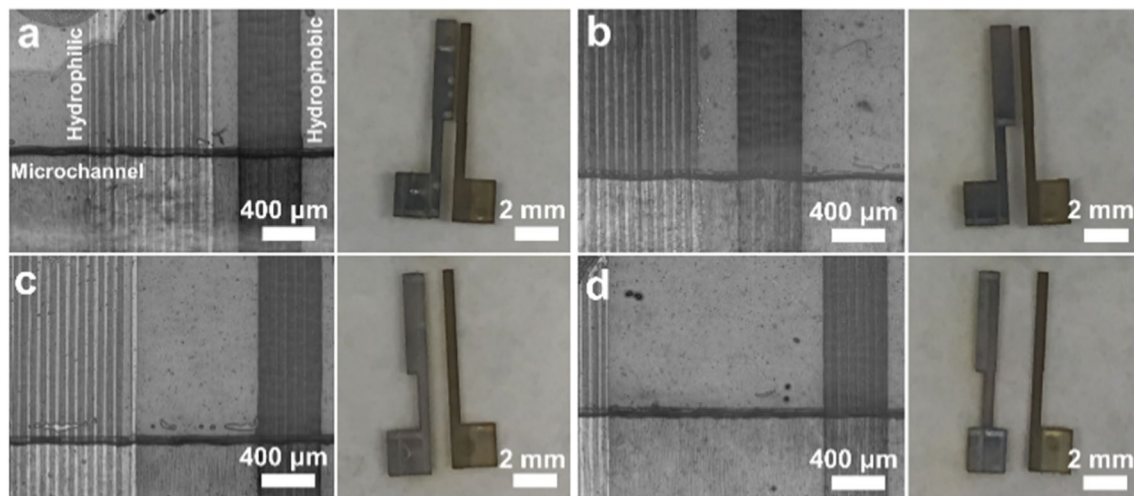
Fig. 4 Electrowetting valves with increasing electrode spacings. (Left) Optical microscopy images of completed valves and (Right) photos of printed electrowetting electrodes with electrode spacings of **a** 0.2 mm, **b** 0.5 mm, **c** 1 mm, **d** 2 mm
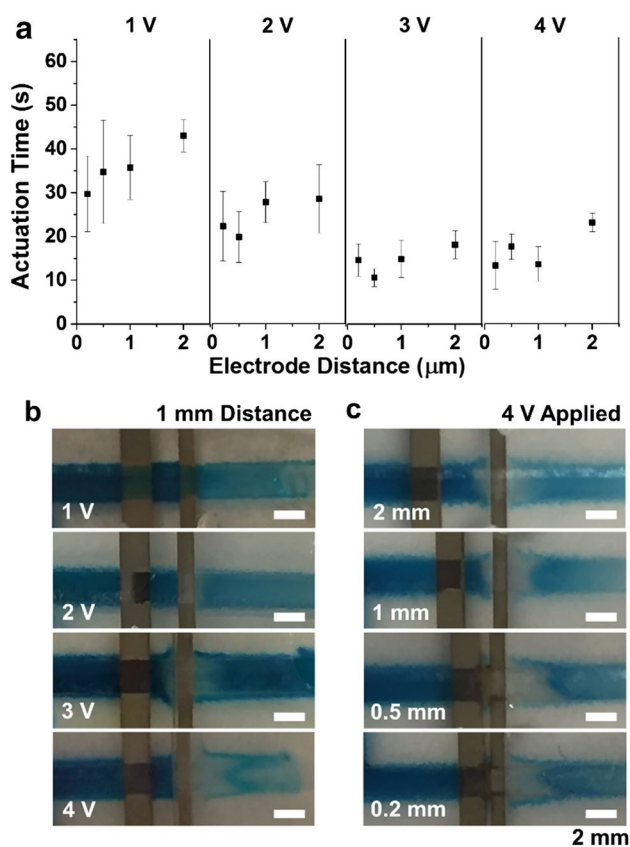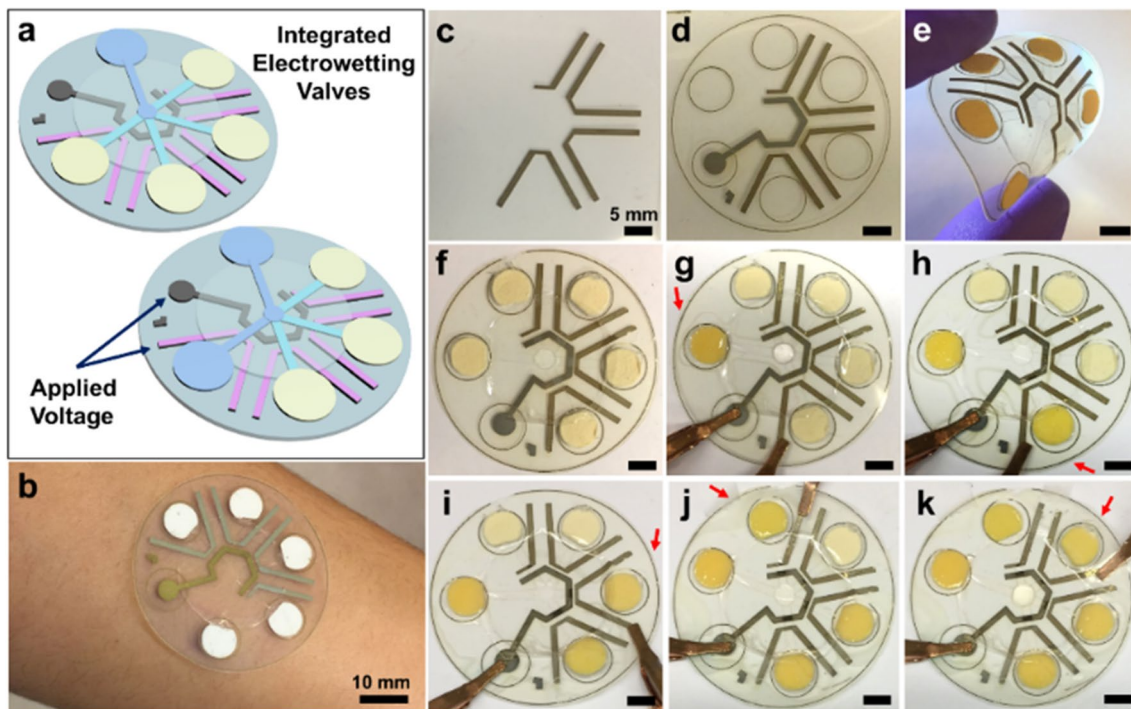

Fig. 5 Electrowetting valve actuation. **a** Relationship between actuation time, applied voltage, and electrode spacing. Error bars represent standard error. Gas bubble formation due to electrolysis of water shown for **b** 1 mm electrode spacing with increasing applied voltage and **c** 4 V applied voltage with decreasing electrode spacing. Scale bars are 2 mm

electrode and a positive to the hydrophilic electrode. This setup allows for reductive desorption to occur between the silver electrode and PFDT monolayer, resulting in a rapid actuation time (Love et al. 2005). Additionally, electrowetting valves demonstrating fluid retention times of 6 h were actuated within expected time ranges using 1 V and 3 V and shown in Fig. S9.

Statistical analysis was performed on valve actuation times using a two-way analysis of variance (ANOVA) at a 95% confidence interval. Two factors, voltages (1, 2, 3, 4 V) and electrode spacings (0.2, 0.5, 1, 2 mm), were examined with four replicates per treatment. As shown in Fig. 5a, the applied voltage showed a significant effect on the actuation times [F $(3,48) = 10.4$, $p < 0.01$]. Using a Tukey's *post-hoc* test, an applied voltage of 1 V resulted in longer actuation times compared with higher voltages (see Fig. S10). The electrode spacing [F$(3,48) = 1.55$, $p = 0.2$] and interaction between factors [F$(9,48) = 2.53$, $p = 0.9$] resulted in no significant effect on actuation time. Therefore, the applied voltage, and not electrode spacing, was a critical factor that influenced the time required to actuate the valve, especially at low voltages. Actuation averages were 17 ± 8 s for 4 V, 14 ± 7 s for 3 V, 30 ± 13 s for 2 V, and 40 ± 16 s for 1 V.

An important consideration for the integration of electrowetting valves into point-of-care sweat sensing devices is that sweat is composed of 99% water (Bariya et al. 2018), and the electrolysis of water occurs at 1.23 V, forming oxygen and hydrogen gas (Rossmeisl et al. 2005). Using applied voltages lower than the electrolysis of water prevents the immediate decomposition of the water in sweat and potential damage to key biomarkers following valve actuation. For example, an actuation voltage of 1 V should be used to prevent oxidation of Cl− within sweat (Haynes 2012).

Fig. 6 Wearable electrowetting valve device. **a** Schematic of electrowetting valve device before and after actuation of first valve. **b** Optical image of device placed on arm. Scale bar is 10 mm. **c** Printed hydrophobic electrodes and **d** hydrophilic electrodes. **e, f** Assembled electrowetting valve device. **g–k** Artificial perspiration pipetted into inlet and valves are actuated at 3 V with at 10-min intervals. Scale bars for **c–k** are 5 mm

This gas formation is evident to the right of the hydrophobic electrode for voltages of 2, 3, and 4 V, as shown in Fig. 5b, c. Increased gas formation was noticeable for higher applied voltages (2 vs. 4 V in Fig. 5b) and smaller electrode spacings (2 vs. 0.2 mm in Fig. 5c). As expected, an applied voltage of 1 V as shown in Fig. 5b demonstrated no gas formation. A secondary benefit of utilizing low voltages is the lower power requirement needed from the external battery source to actuate the valves. For sweat sensing, a voltage of 1 or 2 V with any electrode spacing is recommended when low voltage and power are required, and 3 V or 4 V with any electrode spacing for when rapid valve actuation is required.

3.4 Electrowetting valve integration

The electrowetting valve was designed specifically for integration within a microfluidic wearable device for sweat sensing. Multiple electrowetting valves were incorporated together using consolidated connectors to increase fabrication time, decrease ink consumption, and minimize the footprint of the valving mechanism for the microfluidic device. A single hydrophilic electrode was examined for actuation of multiple electrowetting valves, compared with using an individual hydrophilic electrode per valve. As shown in Fig. S11, four electrowetting valves were inkjet-printed using

a single hydrophilic electrode with electrode spacings of 0.5 mm and was successfully actuated using 4 V with 10 min intervals between each valve actuation. As a note, a single hydrophobic electrode for multiple valves would result in reductive desorption of the monolayer and decreased fluid retention time and would not be recommended. Therefore, the overall dimensions of the connectors needed for electrowetting valves can be minimized using a single hydrophilic electrode for multiple valves.

Electrowetting valves were then integrated into a proof-of-concept wearable device, as shown in Fig. 6. Four electrowetting valves were constructed with 0.5 mm electrode spacings and fabricated equidistant around a central inlet of 3 mm diameter, leading to absorbent pads at the device perimeter. Here, the absorbent pads serve as a visual representation of sweat collection and could be used as colorimetric sensors, but are not necessary for electrowetting valve integration into a sweat sensing device (Bandodkar et al. 2019; Zhang et al. 2019). One single hydrophilic electrode was printed for all four valves as shown in Fig. 6d. In Fig. 6h, i, artificial perspiration without dye was pipetted into the microfluidic inlet and the electrowetting valves were actuated at 10 min intervals. An actuation voltage of 3 V was chosen to allow for rapid actuation, as shown in Fig. 5a. The valves were actuated by applying voltage between the

single hydrophilic electrode and each hydrophobic electrode leading to a valve. The silver connectors for the electrowetting valves were arranged for simple incorporation with a coin cell battery and electric switches for future designs. The overall device had a diameter of 38 mm and a thickness of ~ 0.25 mm.

4 Conclusions

In this work, we have demonstrated the development of wearable electrowetting valves for integration with sweat sensing devices. These valves were fabricated using silver nanoparticle-based ink printed onto a hydrophilic PET substrate for fast capillary-driven flow. The microfluidic system is completed using an inexpensive PSA layer and a medical-grade adhesive for conformal skin contact. Building on previous electrowetting valve concepts, we have shown increased fluid retention times of over 9 h due to improved print quality, high-resolution electrode spacing of 0.2 mm, and reliable low-voltage actuation at 1 V, preventing the electrolysis of water. We further demonstrated the application of electrowetting valves within a proof-of-concept wearable microfluidic patch with sequential valve actuation and fluid collection at well-defined time points. In this way, wearable electrowetting valves offer an inexpensive, printed, and user-friendly method for on-demand sweat collection, leading to improved personal monitoring opportunities.

Compliance with ethical standards

Conflicts of interest There are no conflicts to declare.

References

Alizadeh A, Burns A, Lenigk R et al (2018) A wearable patch for continuous monitoring of sweat electrolytes during exertion. Lab Chip 18:2632–2641. https://doi.org/10.1039/C8LC00510A

Anastasova S, Crewther B, Bembnowicz P et al (2017) A wearable multisensing patch for continuous sweat monitoring. Biosens Bioelectron 93:139–145. https://doi.org/10.1016/j.bios.2016.09.038

Atabakhsh S, Jafarabadi Ashtiani S (2018) Thermal actuation and confinement of water droplets on paper-based digital microfluidics devices. Microfluid Nanofluidics 22:1–9. https://doi.org/10.1007/s10404-018-2060-6

Baker LB (2017) Sweating rate and sweat sodium concentration in athletes : a review of methodology and intra/interindividual variability. Sport Med 47:111–128. https://doi.org/10.1007/s40279-017-0691-5

Bandodkar AJ, Gutruf P, Choi J et al (2019) Battery-free, skin-interfaced microfluidic/electronic systems for simultaneous electrochemical, colorimetric, and volumetric analysis of sweat. Sci Adv 5:1–16. https://doi.org/10.1126/sciadv.aav3294

Bandodkar AJ, Wang J (2014) Non-invasive wearable electrochemical sensors: a review. Trends Biotechnol 32:363–371. https://doi.org/10.1016/j.tibtech.2014.04.005

Bariya M, Nyein HYY, Javey A (2018) Wearable sweat sensors. Nat Electron 1:160–171

Chandekar A, Sengupta SK, Whitten JE (2010) Thermal stability of thiol and silane monolayers: a comparative study. Appl Surf Sci 256:2742–2749. https://doi.org/10.1016/j.apsusc.2009.11.020

Chen J, Zhou Y, Wang D et al (2015) UV-nanoimprint lithography as a tool to develop flexible microfluidic devices for electrochemical detection. Lab Chip 15:3086–3094. https://doi.org/10.1039/C5LC00515A

Choi J, Bandodkar AJ, Reeder JT et al (2019) Soft, skin-integrated multifunctional microfluidic systems for accurate colorimetric analysis of sweat biomarkers and temperature. ACS Sensors 4:379–388. https://doi.org/10.1021/acssensors.8b01218

Coyle S, Morris D, Lau KT, et al (2009) Textile sensors to measure sweat pH and sweat-rate during exercise. In: Pervasive Comput Technol Heal 2009 Pervasive Health 2009 3rd Interntional Conference 4–9. https://doi.org/10.4108/ICST.PERVASIVEHEALTH2009.5957

Di QT, Zhang H, Liang XL, et al (2015) Electrowetting display pixels fabricated by nanoimprint lithography. Int Conf Appl Sci Eng Innov 495–501

Gao W, Emaminejad S, Nyein HYY et al (2016) Fully integrated wearable sensor arrays for multiplexed in situ perspiration analysis. Nature 529:509–514. https://doi.org/10.1038/nature16521

Guo ZH, Jiao YC, Wang HL et al (2019) Self-powered electrowetting valve for instantaneous and simultaneous actuation of paper-based microfluidic assays. Adv Funct Mater 29:1–7. https://doi.org/10.1002/adfm.201808974

Haynes W (2012) CRC handbook of chemistry and physics (92 ed). CRC Press, New York, pp 5–80

He F, Grimes J, Alcaine SD, Nugen SR (2014) A hybrid paper and microfluidic chip with electrowetting valves and colorimetric detection. Analyst 139:3002–3008. https://doi.org/10.1039/c3an01516e

He F, Nugen SR (2014) Automating fluid delivery in a capillary microfluidic device using low-voltage electrowetting valves. Microfluid Nanofluidics 16:879–886. https://doi.org/10.1007/s10404-013-1317-3

Heikenfeld J (2016) Non-invasive analyte access and sensing through eccrine sweat: challenges and outlook circa 2016. Electroanalysis. https://doi.org/10.1002/elan.201600018

Hendriks BHW, Kuiper S, Van As MAJ et al (2005) Electrowetting-based variable-focus lens for miniature systems. Opt Rev 12:255–259. https://doi.org/10.1007/s10043-005-0255-z

Jadoon S, Karim S, Akram MR et al (2015) Recent developments in sweat analysis and its applications. Int J Anal Chem 2015:1–7. https://doi.org/10.1155/2015/164974

Kim SB, Koo J, Yoon J et al (2020) Soft, skin-interfaced microfluidic systems with integrated enzymatic assays for measuring the concentration of ammonia and ethanol in sweat. Lab Chip 20:84–92. https://doi.org/10.1039/c9lc01045a

Koh A, Kang D, Xue Y et al (2016) A soft, wearable microfluidic device for the capture, storage, and colorimetric sensing of sweat. Sci Transl Med 8:1–14. https://doi.org/10.1126/scitranslmed.aaf2593

Koo CKW, He F, Nugen SR (2013) An inkjet-printed electrowetting valve for paper-fluidic sensors. Analyst 138:4998–5004. https://doi.org/10.1039/c3an01114c

Liu H, Dharmatilleke S, Maurya DK, Tay AAO (2010) Dielectric materials for electrowetting-on-dielectric actuation. Microsyst Technol 16:449–460. https://doi.org/10.1007/s00542-009-0933-z

Love JC, Estroff LA, Kriebel JK et al (2005) Self-assembled monolayers of thiolates on metals as a form of nanotechnology. Chem Inform. https://doi.org/10.1002/chin.200532281

Mach P, Krupenkin T, Yang S, Rogers JA (2002) Dynamic tuning of optical waveguides with electrowetting pumps and recirculating fluid channels. Appl Phys Lett 81:202–204. https://doi.org/10.1063/1.1491608

Merian T, He F, Yan H et al (2012) Development and surface characterization of an electrowetting valve for capillary-driven microfluidics. Colloids Surf Physicochem Eng Asp 414:251–258. https://doi.org/10.1016/j.colsurfa.2012.08.020

Moon I, Kim J (2006) Using EWOD (electrowetting-on-dielectric) actuation in a micro conveyor system. Sens Actuators A 130–131:537–544. https://doi.org/10.1016/j.sna.2005.12.016

Mugele F, Baret J-C (2005) Electrowetting: from basics to applications. J Phys Condens Matter 17:R705–R774. https://doi.org/10.1088/0953-8984/17/28/R01

Quilliet C, Berge B (2001) Electrowetting: a recent outbreak. Colloid Interface Sci 6:34–39. https://doi.org/10.1016/S1359-0294(00)00085-6

Rossmeisl J, Logadottir A, Nørskov JK (2005) Electrolysis of water on (oxidized) metal surfaces. Chem Phys 319:178–184. https://doi.org/10.1016/j.chemphys.2005.05.038

Seshadri DR, Li RT, Voos JE et al (2019) Wearable sensors for monitoring the physiological and biochemical profile of the athlete. NPJ Digit Med. https://doi.org/10.1038/s41746-019-0150-9

Shamai R, Andelman D, Berge B, Hayes R (2008) Water, electricity, and between… On electrowetting and its applications. Soft Matter 4:38–45. https://doi.org/10.1039/b714994h

Tohgha UN, Alvino EL, Jarnagin CC et al (2019) Electrowetting behavior and digital microfluidic applications of fluorescent, polymer-encapsulated quantum dot nanofluids. ACS Appl Mater Interfaces 11:28487–28498. https://doi.org/10.1021/acsami.9b07983

Torabinia M, Asgari P, Dakarapu US et al (2019) On-chip organic synthesis enabled using an engine-and-cargo system in an electrowetting-on-dielectric digital microfluidic device. Lab Chip 19:3054–3064. https://doi.org/10.1039/c9lc00428a

Zhang Y, Guo H, Kim SB et al (2019) Passive sweat collection and colorimetric analysis of biomarkers relevant to kidney disorders using a soft microfluidic system. Lab Chip 19:1545–1555. https://doi.org/10.1039/c9lc00103d

Publisher's Note Springer Nature remains neutral with regard to jurisdictional claims in published maps and institutional affiliations.